Journal of Catalysis 408 (2022) 133–141

Contents lists available at ScienceDirect

Journal of Catalysis

journal homepage: www.elsevier.com/locate/jcat

Borosilicate zeolite enriched in defect boron sites boosting the low-temperature oxidative dehydrogenation of propane

Bin Qiu, Wen-Duo Lu, Xin-Qian Gao, Jian Sheng, Bing Yan, Min Ji, An-Hui Lu *

State Key Laboratory of Fine Chemicals, Liaoning Key Laboratory for Catalytic Conversion of Carbon Resources, School of Chemical Engineering, Dalian University of Technology, Dalian 116024, Liaoning, PR China

ARTICLE INFO

Article history:
Received 26 November 2021
Revised 18 February 2022
Accepted 22 February 2022
Available online 10 March 2022

Keywords:
Boron species
Coordination environment
Dynamic evolution
ODHP
Propylene

ABSTRACT

Borosilicate zeolites are the active catalysts in oxidative dehydrogenation of propane (ODHP), which provide an ideal platform to explore the origin of catalytic activity for boron-containing catalysts as well as the construction of highly active boron centers. Herein, we report that the incompletely crystallized MFI-type borosilicate zeolite catalyst displays extraordinary performance in ODHP, exhibiting an olefin productivity of 4.75 $g_{olefin}\ g_{cat}^{-1}\ h^{-1}$ under low reaction temperature (445 °C) and high weight-hour-space-velocity (WHSV, 37.6 $g_{C3H8}\ g_{cat}^{-1}\ h^{-1}$). A combination of solid-state NMR, dual-beam FTIR, and *in-situ* DRIFT measurements reveal that the boron species are anchored to the zeolite matrix in the form of open coordination. Meanwhile, the ample Si—OH groups on the surface facilitate the formation of hydrogen bonds with the B—OH in defective boron species and inhibit the excessive leaching of boron. During the ODHP process, the isolated boron species would dynamically transform into aggregated ones, being closely related to the increased catalytic activity. The B—OH groups in aggregated BO_x species that hydrogen bond with adjacent Si—OH groups are identified as the active center and high efficiency in catalyzing ODHP reaction at low temperature.

1. Introduction

Boron-containing materials generally showed immense potential in oxidative dehydrogenation of propane owing to their superior catalytic activity and high selectivity to olefin, particularly by avoiding the deep oxidation reaction of olefin [1–6]. The oxygenated boron sites at the surfaces of the *h*-BN and other bulky and supported boron-containing catalysts are the origin for catalyzing ODH reactions [1–14]. A variety of strategies have been explored to maximize the number of oxygen-containing boron species to enhance the catalytic performance, such as Na-assisted high-temperature steam activation [1,7], nano-structural engineering, [15–17] and synthesis of high surface area catalysts [6,12,14,18]. Nevertheless, increasing boron loading for supported catalysts is an straightforward route to create more active sites for the ODH reactions [11,12,19,20]. Hence, it is highly desirable to establish a way to prepare boron-containing catalysts with well-dispersed and accessible active boron species.

Borosilicate zeolites with homogeneous distribution of boron have been proved as the promising catalyst in ODHP reaction and the micro-environment of boron species is the dominant factor for the catalytic properties [14,21]. The isolated $B(OSi)_3$ units that are fully incorporated into the zeolite framework are confirmed inactive for ODHP reaction over B-MWW zeolite [22]. On the contrary, the defect boron sites are of the essence in catalyzing the ODHP reaction, and the aggregated boron species are more efficient in C–H bond activation of propane than the isolated species [14,22]. Lately, the isolated boron (—B[OH...O(H)—Si]$_2$) in borosilicate MFI-type zeolite shows superior durability with olefin productivity of 0.2 $g_{olefin}\ g_{cat}^{-1}\ h^{-1}$, and the hydrogen bond formed between B—OH with adjacent Si—OH facilitates the synergistic conversion of oxygen and propane [21]. While a higher reaction temperature (up to 560 °C) is required to achieve substantial olefin productivity over such isolated boron sites. Our previous work shows that the boroxol ring and the tri-coordinated planar $BO_{3/2}$ species in BOS (B_2O_3/SBA-15) catalysts are responsible for the low-temperature ODHP reaction and boron sites with more OH groups are easier to dehydrogenate by dioxygen [12]. In the view of the micro-environment of boron species on the zeolite catalysts, enabling boron species to be uniformly anchored to hydroxyl-rich MFI-type zeolite matrix in oligomeric form may be a feasible way to construct highly active boron centers.

In this work, a series of boron-containing MFI-type zeolite (BMFI) catalysts with different crystallinity and well-dispersed boron species were prepared, and investigated for catalyzing the

* Corresponding author.
E-mail address: anhuilu@dlut.edu.cn (A.-H. Lu).

https://doi.org/10.1016/j.jcat.2022.02.017
0021-9517/

ODHP reaction. The crystallinity was regulated by adjusting the hydrothermal synthesis conditions. It turned out to be that the catalysts with low crystallinity exhibited superior activity and higher productivity of olefin at low temperature. Structure characterizations revealed that the incomplete crystallization could enrich the defect boron sites with hydrogen bonded to adjacent silanols, which were responsible for the superior catalytic activity of the BMFI catalysts.

2. Experimental methods

2.1. Synthesis of BMFI catalysts

The BMFI zeolites were synthesized according to an earlier report with slight modifications [23]. 0.433 g boric acid (Sinopharm) was dissolved in 4.8 g aqueous solution of tetrapropylammonium hydroxide (TPAOH, 25 wt%, Guangfu) and 24 mL deionized water with stirring at room temperature. Then, 2.5 g nano fumed silica (Aladdin) was slowed added to the mixture and strongly stirred for an hour to obtain a gel with a molar composition of $1SiO_2$: $0.084B_2O_3$: 0.1TPAOH: $36H_2O$. The gel was sealed into a 50 mL Teflon-lined stainless-steel autoclave and subjected to hydrothermal treatment at 150 °C statically for several days to obtain the zeolites with different crystallinity. After cooling down to room temperature, the product was filtered, dried, and finally calcined at 550 °C in air for 6 h to remove the templating agent. The samples were labeled as BMFI-x, x for the time in hydrothermal treatment (days). The BMFI-3.0-AT was prepared by stirring 500 mg BMFI-3.0 in 10 mL nitric acid (15 mol/L) at 80 °C for 5 h. After cooling down to room temperature, the product was filtered, washed, dried at 120 °C, and finally calcined at 550 °C in air for 2 h.

2.2. Catalyst characterizations

The actual boron content of the zeolites was measured by inductively coupled plasma optical emission spectroscopy (ICP-OES) on Optima2000DV. Before the measurements, the sample (10 mg) was dissolved by hydrochloric acid (1 mL) and hydrofluoric acid (1 mL) mixed solution in a Teflon-lined autoclave at 150 °C for 1.5 h. After evaporating up the solution that contained hydrochloric acid and hydrofluoric acid, we repeatedly added deionized water into the Teflon container and then collected the solution into a polypropylene volumetric flask, finally fixed the solution volume as 25 mL.

The powder X-ray diffraction (XRD) was recorded on PANalytical X'Pert3 Powder diffractometer using Cu Kα radiation (λ = 0.15 406 nm). The zeolite powder was placed inside a quartz-glass sample holder for testing. The tube voltage was 40 kV, and the current was 40 mA, and the relative crystallinity of BMFI was calculated based on the area of the peaks of angle 2θ = 22–25°.

N_2 adsorption–desorption isotherms were measured with an ASAP 3000 sorption analyzer (Micromeritics). Prior to the measurement, the sample was degassed by evacuation at 200 °C for 4 h. The Brunauer-Emmett-Teller (BET) method was used to calculate the specific surface area (S_{BET}). Total pore volume (V_{total}) was calculated from the amount of gas adsorbed at a relative pressure P/P_0 of 0.99. Micropore volume (V_{micro}) was calculated using the t-plot method.

Fourier transform infrared spectroscopy (FTIR) spectra were recorded on a Nicolet 6700 FT-IR spectrometer equipped with a mercury cadmium telluride (MCT) detector. The evolutions in the hydroxyl regions under different temperatures were monitored by dual-beam Fourier transform infrared spectrometry (DB-FTIR) with a Nicolet 10 FTIR spectrometer. The spectra were processed by subtracting from the measured sample spectra a background spectrum recorded in an empty IR cell in the absence of the catalyst. *In-situ* Diffuse Reflectance Infrared Fourier Transform (DRIFT) spectra were collected on a Bruker 70 V spectrometer equipped with an *in-situ* reaction cell (HARRICK) and MCT detector. The catalyst powder (~30 mg) was placed in the cell and pretreated at 500 °C for 3 h in a flow of 30 vol% O_2/N_2. Subsequently, the sample was maintained at 450 °C in flowing $C_3H_8/O_2/N_2$ (volume ratio of 1:1.5:3.5) gas mixture. The evolution of surface species was monitored by IR by averaging 256 scans at a resolution of 4 cm^{-1}.

^{11}B MAS NMR spectra were recorded on an Agilent DD2-500 MHz spectrometer with an 11.7 T magnet, using a 4-mm MAS NMR probe with a spinning rate of 10 kHz. The spectra were acquired with 600 scans per increment, a recycle delay of 3 s. The pulse length and power were 0.425 μs and 53. Chemical shifts were referenced to a 1 M H_3BO_3 aqueous solution at 19.6 ppm. The DMFIT program was used to deconvolute the spectra and fit the peaks [24]. The peak areas represented the number of nuclear spins, i.e., the content of corresponding B species; therefore, the relative amount of B species in each spectrum could be derived. The BMFI catalysts were stored after reactions under an inert atmosphere and packed into NMR rotors, and then conducted measurements at room temperature.

^{1}H MAS NMR experiments were carried out at 499.8 MHz using a 4 mm MAS NMR probe with a spinning rate of 10 kHz, 64 scans, and 4 s pulse delay. The pulse length and power were 2.6 μs and 61. Hexafluoroisopropanol was used as the standard sample for ^{1}H MAS NMR quantification. The chemical shifts were referenced to tetramethylsilane. Prior to measurement, the sample was dehydrated at 400 °C for 10 h at 10^{-4} Pa and then transferred to a 4 mm MAS rotor in a glove box without exposure to air.

2.3. Catalytic reaction

Selective oxidation of propane studied in a fixed bed reactor (I. D. = 8 mm, length = 42 cm) packed with 50 mg catalyst (the height of catalyst bed is ~3 mm) and heated to 400–550 °C under atmospheric pressure. The feed gas contains $C_3H_8/O_2/N_2$ with a volume ratio of 1:1.5:3.5 at a fixed total flow rate of 96 mL/min. Before reaction, each BMFI catalyst was pretreated to stabilize the coordination environment of boron species under reaction conditions. Reactants and products were analyzed using an online gas chromatograph (Techcomp, GC 7980) equipped with a GDX-102 and molecular sieve 5A column. A TCD was used to detect O_2, N_2, C_3H_8, C_3H_6, C_2H_4, CO, and CO_2. The conversion was defined as the number of moles of carbon converted divided by the number of moles of carbon present in the feed. Selectivity was defined as the number of moles of carbon in the product divided by the number of moles of carbon reacted. The turnover frequency (TOF) was calculated based on the hypothesis that $B[3]^a$ were the active sites. The quantity of $B[3]^a$ species was calculated from the results of ^{11}B MAS NMR spectra and ICP-OES. The carbon balance was checked by comparing the number of moles of carbon in the outlet stream to the number of moles of carbon in the feed. Under our typical evaluating conditions, the carbon balance was generally higher than 95%.

The mass and heat transfer diffusion limitation have been ruled out for the highest propane reaction rate based on Weisz-Prater criterion and Mears criterion [25,26] as shown in Supplementary Material.

The reaction rate of propane $r(C_3H_8)$ and TOF were calculated as follows:

$$r(C_3H_8) = F(C_3H_8) \times X(C_3H_8)/[(m(\text{cat}) \times C(B)/M(B)].$$

$$\text{TOF}\ (h^{-1}) = F(C_3H_8) \times X(C_3H_8) / [(m(\text{cat}) \times C(B_{\text{active}}) / M(B)].$$

where $F(C_3H_8)$ is the molar flow rate of C_3H_8 at the inlet of the reactor, $X(C_3H_8)$ represents the conversion of C_3H_8, m(cat) is the weight of catalyst, C(B) is the content of boron atoms on the catalyst, $C(B_{active})$ is the content of active boron atoms on the catalyst, and M(B) is the molar mass of boron atom.

3. Results and discussion

3.1. Structure and property of BMFI catalysts

The structural variations of BMFI catalysts were characterized using different means. The XRD patterns of the BMFI catalysts crystallized at different periods of time after calcination were shown in Fig. 1a. All samples exhibited typical diffraction peaks at 2θ of 23.1, 23.3, 23.7, 24.0, and 24.4°, indicating the strong characteristic of MFI framework structure [23]. No additional peaks of B_2O_3 were observed, revealing the uniform dispersion of boron species. The relative crystallinity of BMFI catalyst was calculated based on the areas of peaks ranging from 22 to 25° in the XRD pattern. Highly crystalline BMFI catalyst was obtained at long periods of crystallization time. For instance, three days of crystallization afforded 16% of relative crystallinity and it increased to 49% when the crystallization time was extended to 3.5 days. The relative crystallinity was sharply increased and remained constant when the crystallization process lasted for more than 4 days (Fig. 1b). Fig. 1c showed the IR spectra of as-synthesized samples obtained at different crystallization times. The peak at ~926 cm^{-1} can be attributed to the Si—O—B vibration [27], and the peak that appeared at ~1405 cm^{-1} was attributed to the asymmetric stretching vibration of BO_3 unit [28] which can be the evidence for the incorporation of boron atoms into the zeolite matrix. As shown in Fig. 1d and Table S1, the textural properties of BMFI catalysts were highly dependent on the relative crystallinity. The apparent surface area of the zeolite samples varied from 163 to 456 m^2/g. High crystallinity afforded a large micropore area, confirming the crystalline structure was gradually assembled with time.

3.2. Catalytic performance of BMFI catalysts

The catalytic performance of BMFI catalysts for ODHP reaction was conducted in an atmospheric fixed-bed reactor at a temperature range of 400–550 °C. There was almost no measurable conversion of propane in empty reactor without inert solids under identical reaction conditions. Moreover, the effect of the remaining volume of the reactor was tested and we found there was no observed difference in reaction rate of propane, indicating that the catalytic activity was originated from the BMFI catalysts (Fig. S1). As shown in Fig. 2, the BMFI catalysts with the crystallinity of 16% (BMFI-3.0) to 49% (BMFI-3.5) were highly active in ODHP reaction at the temperature above 400 °C and maintained

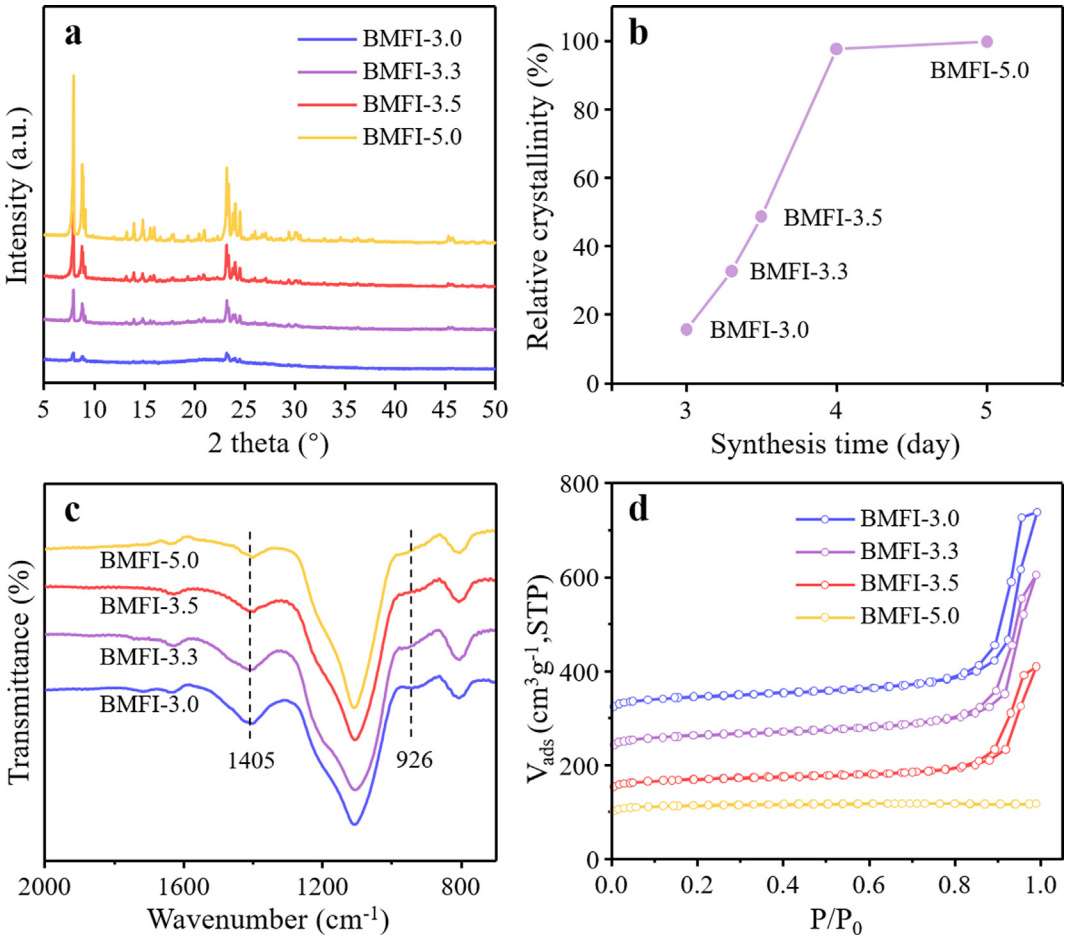

Fig. 1. (a) XRD patterns and (b) relative crystallinity of the BMFI catalysts synthesized over different periods. The crystallinity of the solid product was calculated based on the areas of the peaks ranging from 22° to 25° and the BMFI zeolite synthesized at 150 °C for 5 days was chosen as the standard for the calculation. (c) FT-IR spectra and (d) N_2 sorption isotherms of BMFI catalysts. N_2 sorption isotherms of BMFI-3.0, BMFI-3.3, and BMFI-3.5 were vertically shifted an additional 300, 200, and 100 $cm^3\ g^{-1}$ (STP) for easy view.

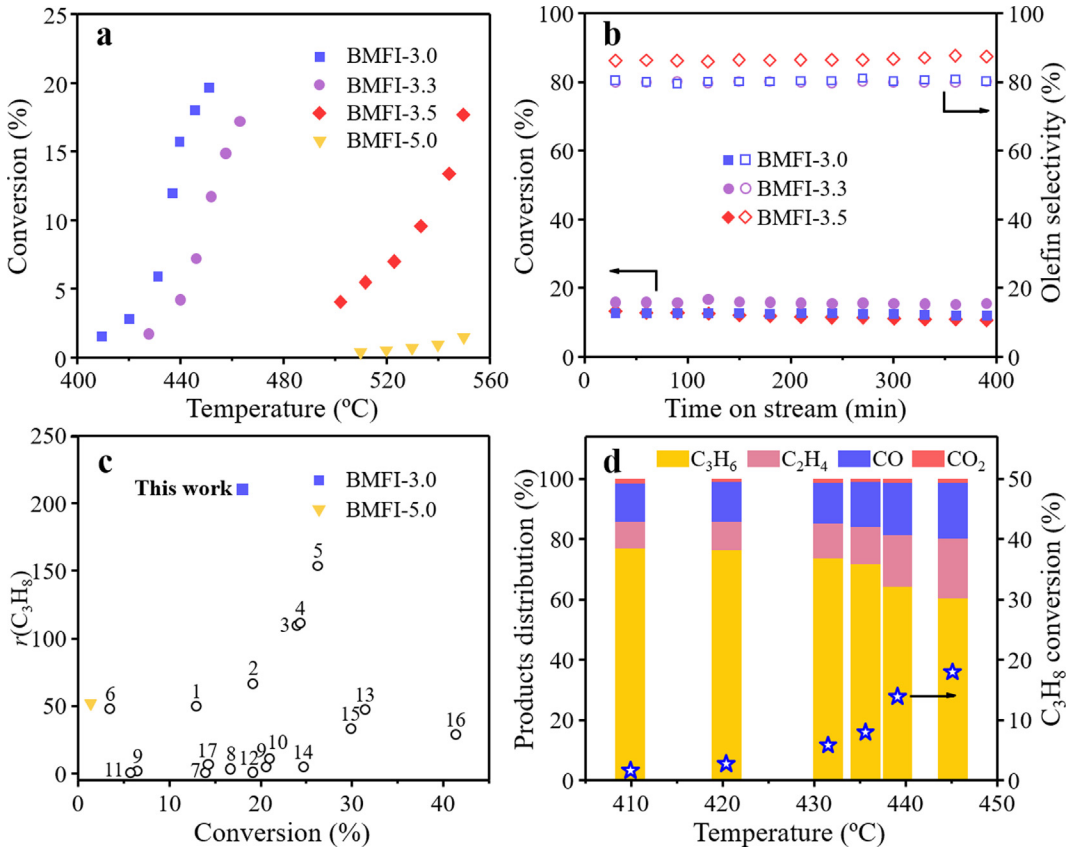

Fig. 2. (a) Influence of temperature on the propane conversion over BMFI catalysts. (b) Time on stream profiles of propane conversion and olefin (C_3H_6 + C_2H_4) selectivity over BMFI-3.0 (440 °C), BMFI-3.3 (460 °C), and BMFI-3.5 (540 °C) catalysts. (c) Comparison of reaction rate of propane for ODHP as a function of C_3H_8 conversion over BMFI and several representative catalysts (Table S2). The units of $r(C_3H_8)$ are $mol_{C3H8}\ mol_{metal}^{-1}h^{-1}$ for metal oxide catalysts (No. 1–6) and $mol_{C3H8}\ mol_{boron}^{-1}h^{-1}$ for boron-containing catalysts (No. 7–17). (d) Products distribution and conversion of BMFI-3.0 catalyst. Reaction condition: m_{cat} = 50 mg, gas feed: $C_3H_8/O_2/N_2$ with a molar ratio of 1/1.5/3.5; flow rate of 96 mL/min.

stability in catalytic activity and zeolite structure during the test (Fig. 2a, b, Fig. S2). The BMFI-3.0 shows a propane conversion of 18.0% at 445 °C. Raising the crystallinity from 16% (BMFI-3.0) to 33% (BMFI-3.3), the propane conversion decreased from 18.0% to 7.1% at 445 °C. While with further increase of crystallinity to 49% (BMFI-3.5) and 100% (BMFI-5.0), the propane conversion greatly decreased to 5.4% and 0.4% at 510 °C, showing the significant influence of the crystallinity toward the catalytic activity. To reach the same propane conversion of ~18%, the BMFI-3.5 catalyst required a reaction temperature of 550 °C, while the conversion was only 1.4% for BMFI-5.0 at 550 °C. The apparent activation energies of propane over BMFI catalysts were quite similar (from BMFI-3.0 to BMFI-5.0 were 174, 182, 187, and 178 kJ/mol, respectively), indicating that the active sites of the BMFI catalysts were essentially identical (Fig. S3). Therefore, the stronger response to the temperature for the propane conversion over the BMFI-3.0 catalyst may be correlated with a large number of active boron species. A large number of active sites involved in the catalysis over the BMFI-3.0 catalyst allowed it to achieve an equivalent conversion at lower reaction temperatures (at least by 100 °C compared to BMFI-3.5 and BMFI-5.0). Moreover, high olefin productivity (4.75 $g_{olefin}\ g_{cat}^{-1}\ h^{-1}$) were obtained for the BMFI-3.0 catalyst at low temperature (445 °C) and high WHSV of 37.6 $g_{C3H8}\ g_{cat}^{-1}\ h^{-1}$ (Table S2). In the view of catalytic efficiency of boron atoms, BMFI-3.0 catalyst exhibited a reaction rate of ~210 $mol_{C3H8}\ mol_{boron}^{-1}\ h^{-1}$ (Fig. 2c, Table S2), which was remarkably higher than that of the reported metal oxide and other boron-based catalysts used in the ODHP process. From the TOF comparison, it could be found that the BMFI-3.0 exhibited highest performance (428 h^{-1} at 445 °C) among the supported boron-based catalysts and borosilicate zeolite catalysts. These results suggested that the boron species on the BMFI-3.0 catalyst possessed higher ability to activate propane, showing excellent catalytic activity at a boron content of only 0.85 wt%.

The products of propane ODH reaction consisted of C_3H_6, C_2H_4, and CO, and a small amount of CO_2 (Fig. 2d). All catalysts exhibited identical trends of the olefin selectivity at the same conversion and slightly decreased with increasing temperature (Fig. S4a). For BMFI-3.0 catalyst, the selectivity of light olefin ($C_{2-3}^{=}$) remained above 80%, e.g., the $C_{2-3}^{=}$ selectivity reached 85.3% at 430 °C ($C_3^{=}$: 73.8%, $C_2^{=}$: 11.5%), 81.3% at 440 °C ($C_3^{=}$: 64.3%, $C_2^{=}$: 17.0%), and 80.4% at 445 °C ($C_3^{=}$: 60.3%, $C_2^{=}$: 20.1%). Except for light olefin, CO was the main C_1 product that may be formed by the gas phase radical reaction through the C-C bond cleavage of propane [29,30]. This deduction could be verified by a control experiment with a feed gas of $C_3H_6/O_2/N_2$, propylene conversion of <4%, only 1/5 of propylene conversion over the catalyst under the same conditions was obtained (Fig. S4b). Therefore, the C_1 product is likely generated from propane other than propylene. Moreover, the influence of WHSV showed that high flow rate contributed to the inhibition of CO_x formation and improved the selectivity of olefin (Fig. S5). This could be attributed to the shortened contact time of reactants under high WHSV and reducing its deep oxidation.

Kinetic experiments were performed to gain insights into the reaction mechanism of propane ODH over the BMFI-3.0 catalyst. The oxygen conversion showed a similar trend to propane with the temperature while exhibiting higher apparent activation

energy of 195 kJ/mol. (Fig. S6a, b). The sample BMFI-3.0 showed about 0.5 dependence with respect to oxygen partial pressure, this meant that the hydrogen abstraction of propane could readily happen after oxygen activation on the BMFI-3.0 catalyst under ODHP conditions (Fig. S6c). It was worth noting that the effect of propane partial pressure was estimated to be 1.54 over BMFI-3.0 catalyst, suggesting a different catalytic behavior compared with *h*-BN and other boron-containing catalysts (Fig. S6d). As known, the ODH reaction catalyzed by boron-based catalysts involved both surface and gas-phase reactions. Moreover, the rate of the homogeneous gas-phase reaction was the function of reaction temperature, i.e. high reaction temperature, high reaction rate. Thus, the low propane reaction order on BMFI-3.0 catalyst may be due to the limited contribution of gas-phase reactions to the ODHP process at low reaction temperature (e.g. 420 °C). This deduction could be verified by the reaction order of propane on the BMFI-5.0 catalyst, which showed a higher value of 1.86 at 540 °C (Fig. S6d). Moreover, compared with the linear correlation between propane conversion and residence time on BMFI-3.0, the propane conversion super-linearly increased with the longer residence time on BMFI-5.0 catalyst (Fig. S7). These results suggested that the surface activation of propane was more favorable during the low-temperature ODHP process over BMFI-3.0 catalyst.

3.3. Evolution of the active boron species

To gain a better understanding of the structure of catalysts and the origin of catalytic activity, solid-state NMR and IR spectroscopy of BMFI-3.0 and BMFI-5.0 catalysts were collected. Fig. 3 showed ^{11}B MAS NMR spectra of BMFI-3.0 and BMFI-5.0 catalysts. The spectra could be classified into three components of trigonal boron species with the chemical shift at ca. 16.8–17.6, 13.9–15.1, and 10.1–11.6 ppm which were accordingly denoted as B[3]^a, B[3]^b, and B[3]^c [11,12,14,22,31,32]. These peaks were characterized by quadrupolar lineshape with a quadrupole coupling constant (C_Q) at 2.3–2.6 MHz [12,32]. The ^{11}B shift isotropic chemical shift of trigonal boron species was found to correlate with the number of B—O—Si bonds that could be used to identify the different boron coordination environments [32,33]. As the previous reports, site B[3]^a could be ascribed to aggregated boron species that were rich in terminal B—OH groups [12,14]. Considering that the catalysts have been calcined at 550 °C, the B[3]^a species may be anchored in the zeolite matrix in the form of boroxol ring or chain-type BO_x which was the preferred structure of aggregated "BO species" at high temperature [11,12,34]. Site B[3]^b was attributed to defect boron species in the framework balanced by single or double hydroxyl groups due to the similar chemical characteristic of B$(OSi)_2(OH)$ and B$(OSi)(OH)_2$ [11,22,31]. Site B[3]^c was attributed to the B$(OSi)_3$ that was fully incorporated into the zeolite framework. The relative abundance of the three types of boron species for BMFI-3.0 and BMFI-5.0 catalysts showed close dependence with crystallinity and their contents were summarized in Table S3. The proposed structure of three types of boron species was shown in Fig. S8.

The increase of crystallinity led to less proportion of defect boron sites in the framework which was characterized by the decrease in the content of B[3]^a and B[3]^b accompanied by the increase in the content of B[3]^c. This indicated that the long hydrothermal synthesis time during the crystallization process led to a high degree of boron anchoring and microporous structure (Figs. 1a,d and 3a,b). In addition, the spent BMFI-3.0 and BMFI-5.0 catalysts showed increased content of defective boron species (B[3]^a + B[3]^b) and a decrease of B[3]^c. Meanwhile, the defective boron species over spent catalysts still showed the correlation with crystallinity, that is, low crystallinity was more favorable for the formation of defective boron sites (Figs. 3c,d; S9). Most likely, there were dynamic transformations among the three trigonal boron species. The saturated coordination B[3]^c has been proved to be

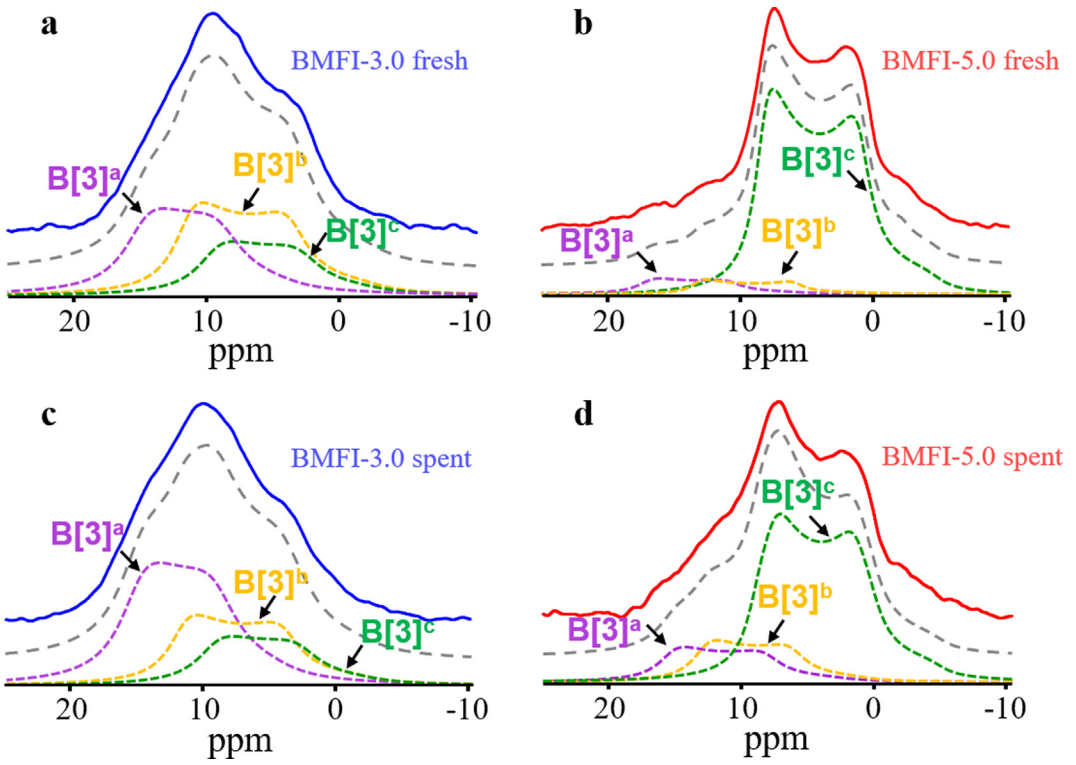

Fig. 3. ^{11}B MAS NMR spectra with an 11.7 T magnet of fresh and spent BMFI catalysts: (a, c) BMFI-3.0, (b, d) BMFI-5.0. The top lines represent the experimental spectra, the gray dashed lines represent the total analytical simulations of the spectra, and the overlapping individual peaks below represent the features of three types of boron species.

inactive in the ODHP reaction, while its conversion to the defective boron species would result in the enhancement of catalytic activity [12,14]. Therefore, the superior catalytic activity of BMFI-3.0 was originated from the abundant of B[3]^{a} and B[3]^{b} species. Considering the decrease in B[3]^{b} content in spent BMFI-3.0 catalyst, the B[3]^{b} species was regarded as the transition species, which was further transformed into B[3]^{a} during the ODHP reaction. Thus, B[3]^{a} should be responsible for catalyzing the ODHP reaction at lower reaction temperature and can be dynamically generated from B[3]^{b} and B[3]^{c}.

^{1}H MAS NMR spectroscopy was additionally used to characterize the hydroxyl groups of BMFI-3.0 and BMFI-5.0 catalysts. As shown in Fig. 4 and Table S4, after deconvolution, six peaks can be identified for both BMFI-3.0 and BMFI-5.0 catalysts. The peaks around 1.9 and 2.2 ppm were respectively assigned to external and internal silanol groups, while the small peak at 2.6 ppm arose from additional Si—OH··· B[3] protons with strong interaction to the framework B[3] units [12,31,35]. The proton form of borosilicate zeolites undergoes B[4] to B[3] transformation upon calcination, which brought about the formation of the internal silanol and isolated B[3] sites. Hence, several works also assigned the peak at 2.2 ppm to the "bridging hydroxyl" sites of Si—OH··· B[3], as its signal weakly associated with B[3] framework sites under different dehydration temperatures [32,36,37]. The ratio of Si—OH··· B[3] and internal silanol in BMFI-5.0 was much higher than that for BMFI-3.0 (37.5% vs 23.7%), it suggested a relatively high proportion of B[3]^{c} on the former catalyst. This was consistent with the results of ^{11}B MAS NMR, that is, higher crystallinity resulted in a higher degree of boron anchoring. The peaks at 3.0, 3.6, and 3.9 ppm could be assigned to the proton in isolated B–OH without hydrogen bond, H-bonded B—OH (B—OH···O—Si), and framework B(OSi)$_2$OH, respectively [12,31,32,37]. The broadened H-bonded proton signal at 3.6 ppm was observed for the BMFI catalysts. It may attribute to the diversity of boron species adjacent to silanol, which included the form of isolated and oligomeric [38]. Among the hydroxyl-containing boron species, isolated B–OH only accounted for ~10% in BMFI-3.0 and BMFI-5.0 catalysts, which suggested a large amount of defective B[3] species were right next to Si—OH groups. After the ODHP test, the signals at 2.2, 3.0, and 3.6 ppm gained intensity due to the hydrolysis of B—O—Si, which was consistent with the results of ^{11}B MAS NMR. It should be noted that the signal at 3.9 ppm was greatly reduced accompanied by the increase in 3.6 ppm. Together with the results of ^{11}B MAS NMR, we can deduce that the transformation of B[3]^{b} to B[3]^{a} occurs, and the resultant B[3]^{a} species was hydrogen-bonded to the adjacent silanol groups.

Fig. 5 presented DB-FTIR spectra for BMFI-3.0 catalysts at different temperatures under O_2/He atmosphere. The isolated Si—OH and B—OH were identified to have characteristic modes at about 3740 and 3700 cm^{-1} (Fig. 5a), confirming the abundance of coordinatively unsaturated sites which was consistent with the results of XRD and ^{11}B MAS NMR [28,39]. In addition, two broad bands at about 3530 and 3675 cm^{-1} were observed for OH groups with hydrogen bonds. The band at 3530 cm^{-1} disappeared at a high temperature of 150 °C and the band at 3675 cm^{-1} decreased intensity with increasing dehydration temperature. The 3530 cm^{-1} may arise from the weak hydrogen-bonded OH groups rather than with water since the absence of water was confirmed by the inexistence of the bending vibration of H_2O at 1630 cm^{-1} [32]. Another broad band around 3675 cm^{-1} decreased in intensity at temperatures of 150 °C and remained nearly constant at 150–450 °C, suggesting there was stable interaction between hydroxyls. To further verify the origin of the interaction at the region of 3530 and 3675 cm^{-1}, the BMFI-3.0 was washed by nitric acid to remove the boron sites, and the corresponding DB-FTIR spectra was shown in Fig. 5b. As a consequence, a significant loss was observed for 3700 cm^{-1}, indicating that almost all boron was removed after nitric acid treatment. Meanwhile, the hydroxyl interaction region at 3530 cm^{-1} disappeared and 3675 cm^{-1} decreased dramatically even at 30 °C, implicating that the boron sites were correlated with the hydroxyl interaction region. Therefore, the band at 3530 cm^{-1} may be due to the weak hydrogen bonds of B—OH with adjacent hydroxyls. Notably, the H_3BO_3 and B_2O_3 showed no absorption band at 3675 cm^{-1}, suggesting the interaction between B—OH groups could be ruled out at the absorption band of 3675 cm^{-1}

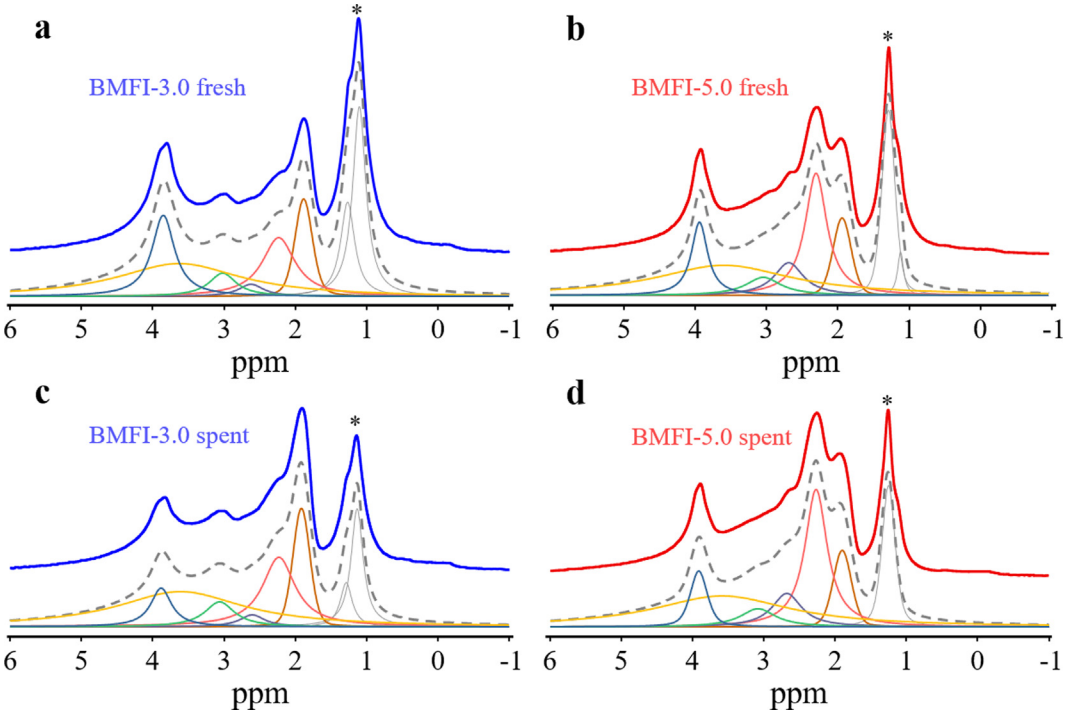

Fig. 4. ^{1}H MAS NMR spectra of fresh and spent BMFI catalysts (a, c) BMFI-3.0 and (b, d) BMFI-5.0 catalysts. The asterisks at 1–1.2 ppm represent the background of signals.

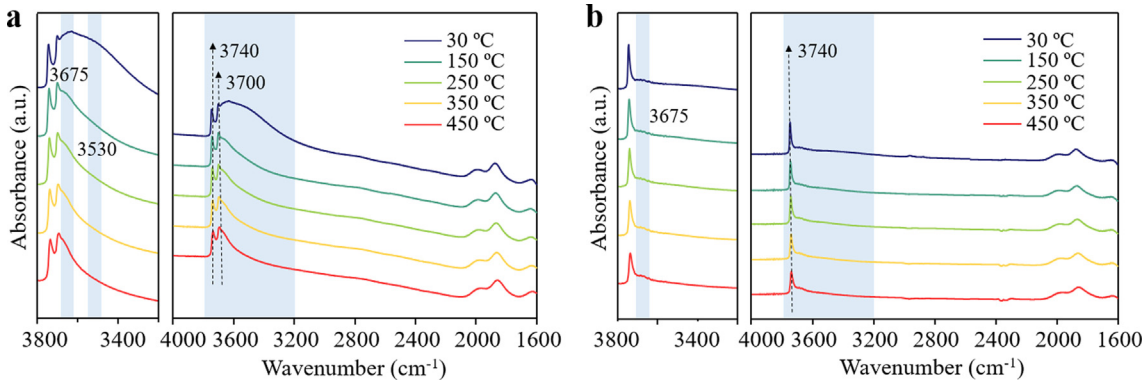

Fig. 5. *In-situ* DB-FTIR spectra of (a) fresh BMFI-3.0 and (b) BMFI-3.0-AT catalysts under O_2/He atmosphere at 30, 150, 250, 350, 450 °C.

[40,41]. Therefore, the band at 3675 cm^{-1} was assigned to the strong interaction between B—OH with adjacent Si—OH, which was consistent with the result in Fig. 4 and earlier reports [32,39,42]. The DB-FTIR spectra of the BMFI-5.0 were shown in Fig. S10. In contrast to the BMFI-3.0 catalyst, both characteristic absorption bands of isolated B—OH and Si—OH were greatly reduced due to the saturated coordination environment. Correspondingly, the loss of the absorption bands at 3675 and 3530 cm^{-1} were also observed which represent the decrease of hydroxyls and hydrogen bonds.

The surface compositions and structure evolution of the BMFI-3.0 catalyst during the reaction were monitored by *in-situ* Diffuse Reflectance Infrared Fourier Transform (DRIFT) spectroscopy. The fresh BMFI-3.0 was purged with O_2/N_2 for 3 h at 500 °C to eliminate molecularly adsorbed H_2O and other absorbates. Then, the sample was further treated under O_2/N_2, C_3H_8/N_2, and $C_3H_8/O_2/N_2$ atmospheres at 450 °C, and the DRIFT difference spectra were shown in Fig. 6. When the catalyst was exposed to O_2/N_2 and C_3H_8/N_2 atmospheres, the surface composition remained unchanged and no propane conversion was detected, which indicated the boron species was stable under the condition of only oxygen or propane and inactive for dehydrogenation in anaerobic conditions (Fig. 6a). With the addition of molecular oxygen in propane ($C_3H_8/O_2/N_2$), the characteristic band of hydroxyl stretching vibration was clearly observed at 3740, 3695, and 3675 cm^{-1} for isolated Si—OH, B—OH [43], and the hydrogen-bonded B–OH. Besides, the strong alkyl stretching signal at 2965 cm^{-1} was attributable to the presence of gas-phase propane [44] (Fig. 6b).

Upon increasing the reaction time, a continuous decrease of the alkyl stretching signal was observed, indicating that there was an activation process at the initial reaction period, during which the catalytic activity gradually enhanced. With the promotion of propane conversion, the ratio of the band intensities at 3740, 3695 and 3675 cm^{-1} increased at first 50 min (Fig. S11a), hinting the hydrolysis of B—O—Si and generated B—OH and Si—OH. After 60 min, an increase in the intensity of the Si—OH groups were still observed, while the formation of B—OH was decreased, as evidenced by the decrease in the intensity of the bands at 3695 and 3675 cm^{-1} (Fig. S11b). Besides, there was a negative broad band at the wavenumber of 3530 cm^{-1}, which indicated the instability of weak hydrogen-bonding hydroxyls under ODH conditions. Considering the enhanced catalytic activity and negligible changes in boron content, the B—OH groups may undergo structural evolution and give rise to more active boron species during this period. As shown in ^{11}B MAS NMR results, the B[3]^a was in aggregated form and increased at the cost of B[3]^b and B[3]^c after ODHP reaction. Therefore, the decrease of B—OH groups was caused by the condensation among B—OH that formed aggregated boron species. The structural evolution of isolated boron to B—O—B oligomers also resulted in the decrease of hydrogen-bonding B—OH groups since the decrease of the proton density in B—O—B oligomers. Moreover, we also noted that the IR signal for Si—OH (3740 cm^{-1}) increased in intensity accompanied with time on stream under ODHP condition (Fig. S12). This feature suggested that there was almost no consumption of Si—OH such as dehydration with B—OH or Si—OH. Therefore, the aggregation of B—OH occurred mainly at the boron site on the zeolite matrix rather than at the Si—OH groups. The abundant Si—OH on the surface were favorable for the formation of B—OH with strong hydrogen bonds, which inhibited excessive leaching of boron and promoted the formation of aggregated boron species on the defective boron sites [21].

These results indicated that the coordination environment of boron species can be regulated by tailoring the zeolite crystallinity,

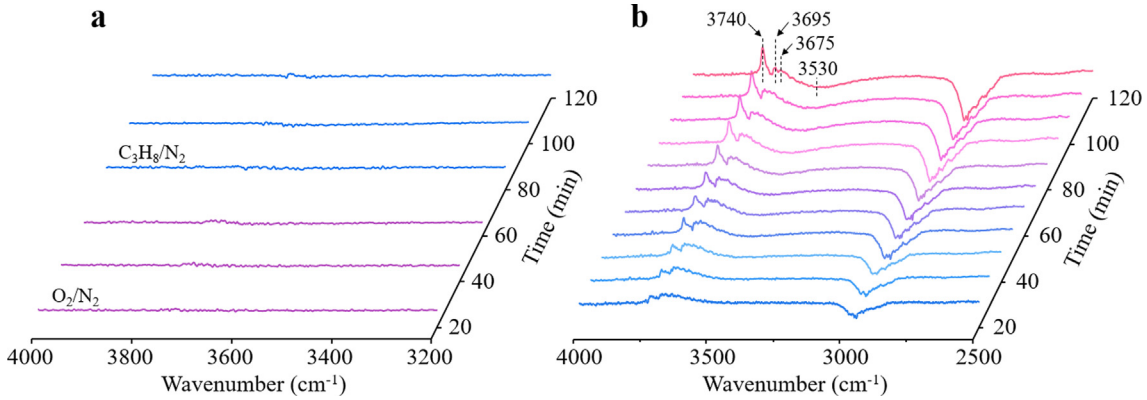

Fig. 6. *In-situ* DRIFT difference spectra of fresh BMFI-3.0 catalyst under (a) O_2/N_2, C_3H_8/N_2 and (b) $C_3H_8/O_2/N_2$ atmosphere at 450 °C.

and the abundant defect boron species could be obtained in zeolite matrix with a low degree of crystallinity. Moreover, the isolated boron sites with defects may serve as the anchor site to promote the formation and stabilization of boron oligomer through the hydrolysis-dehydration process under ODH conditions. It was worth noting that strong interactions present between oligomer boron species and adjacent Si—OH groups in addition to isolated boron species.

For boron-containing catalysts, B—OH groups played a key role in the activation of light alkane [45], and B—O—B oligomers are more active for catalyzing ODH reaction [12,19,20]. High loading of boron is necessary to generate highly active aggregated B—O units which enables the catalyst to exhibit remarkable olefin productivity at low temperatures. In our previous work, 10 wt% B_2O_3 was needed for supported BOS-10 catalyst to highly catalyze the ODHP reaction at the temperature of 450 °C under 9.4 $g_{C3H8}\ g_{cat}^{-1}\ h^{-1}$ [12]. Chen et al. reported boron-hyperdoped silicon catalyst with 25 at % boron concentration exhibited high olefin productivity of 1.97 $g_{olefin}\ g_{cat}^{-1}\ h^{-1}$ under 28.2 $g_{C3H8}\ g_{cat}^{-1}\ h^{-1}$ [19]. In addition, the hydrogen bonds between B—OH and adjacent Si—OH was recently proved to have positive effect in promoting the catalytic activity in ODHP reaction [21]. Similarly, a recent work showed that the hydrogen bond between Hf—OH and Si—OH results in the oxygen atom at Hf—OH being more nucleophilic and facilitated the transfer of a proton to the Lewis basic O atom [38]. In our work, the low crystallinity of the zeolite allowed the boron anchored to the BMFI-3.0 catalyst in an open coordination structure, which promoted the exposure and formation of oligomeric boron species with defects at only 0.85 wt% boron loading. Moreover, the B—OH groups in oligomeric boron species were H-bonded to the adjacent Si—OH groups. Meanwhile, more such species were observed during ODH reaction, suggesting that these species correlated with the catalytic activity. Therefore, the high ODHP activity in BMFI-3.0 most likely resulted from the abundant aggregated defect boron species interacted with adjacent silanols through hydrogen bonds.

4. Conclusions

In this study, we have demonstrated that the relative crystallinity and the coordination environment of the species of BMFI catalysts play essential role in the catalytic activity of ODHP. The catalyst with the crystallinity of 16% exhibited remarkable ODH activity with a propane conversion of 18.0% and an olefin selectivity of 80.4% under a high WHSV of 37.6 $g_{C3H8}\ g_{cat}^{-1}\ h^{-1}$ at 445 °C. Moreover, high olefin productivity of 4.75 $g_{olefin}\ g_{cat}^{-1}\ h^{-1}$ was obtained, which was much higher than most of the previously reported catalysts at the low reaction temperature. Structural characterization revealed that the B—OH in tri-coordinated aggregated BO_x species interacted with adjacent silanols through hydrogen bonds were presently identified as the active sites being responsible for the low-temperature activity and high efficiency in catalyzing ODH of propane. And the defect-rich surface offered an ideal environment for the formation of hydrogen bonds between B—OH and adjacent silanol groups.

Declaration of Competing Interest

The authors declare that they have no known competing financial interests or personal relationships that could have appeared to influence the work reported in this paper.

Acknowledgements

This study was supported by state key program of National Natural Science Foundation of China (21733002), National Key Research and Development Program of China (2018YFA0209404), the Program for Liaoning Innovative Research Team in University (LT2016001).

Appendix A. Supplementary material

Supplementary data to this article can be found online at https://doi.org/10.1016/j.jcat.2022.02.017.

References

[1] L. Shi, D. Wang, W. Song, D. Shao, W.-P. Zhang, A.-H. Lu, Edge-hydroxylated boron nitride for oxidative dehydrogenation of propane to propylene, ChemCatChem 9 (10) (2017) 1788–1793.
[2] J.T. Grant, C.A. Carrero, F. Goeltl, J. Venegas, P. Mueller, S.P. Burt, S.E. Specht, W. P. McDermott, A. Chieregato, I. Hermans, Selective oxidative dehydrogenation of propane to propene using boron nitride catalysts, Science 354 (2016) 1570–1573.
[3] R. Huang, B. Zhang, J. Wang, K.-H. Wu, W. Shi, Y. Zhang, Y. Liu, A. Zheng, R. Schlögl, D.S. Su, Direct insight into ethane oxidative dehydrogenation over boron nitrides, ChemCatChem 9 (17) (2017) 3293–3297.
[4] J.T. Grant, W.P. McDermott, J.M. Venegas, S.P. Burt, J. Micka, S.P. Phivilay, C.A. Carrero, I. Hermans, Boron and boron-containing catalysts for the oxidative dehydrogenation of propane, ChemCatChem 9 (19) (2017) 3623–3626.
[5] B. Yan, W.-C. Li, A.-H. Lu, Metal-free silicon boride catalyst for oxidative dehydrogenation of light alkanes to olefins with high selectivity and stability, J. Catal. 369 (2019) 296–301.
[6] W.-D. Lu, X.-Q. Gao, Q.-G. Wang, W.-C. Li, Z.-C. Zhao, D.-Q. Wang, A.-H. Lu, Ordered macroporous boron phosphate crystals as metal-free catalysts for the oxidative dehydrogenation of propane, Chin. J. Catal. 41 (2020) 1837–1845.
[7] L. Shi, B. Yan, D. Shao, F. Jiang, D. Wang, A.H. Lu, Selective oxidative dehydrogenation of ethane to ethylene over a hydroxylated boron nitride catalyst, Chin. J. Catal. 38 (2017) 389–395.
[8] A.M. Love, B. Thomas, S.E. Specht, M.P. Hanrahan, J.M. Venegas, S.P. Burt, J.T. Grant, M.C. Cendejas, W.P. McDermott, A.J. Rossini, I. Hermans, Probing the transformation of boron nitride catalysts under oxidative dehydrogenation conditions, J. Am. Chem. Soc. 141 (1) (2019) 182–190.
[9] Y. Zhou, J. Lin, L. Li, X. Pan, X. Sun, X. Wang, Enhanced performance of boron nitride catalysts with induction period for the oxidative dehydrogenation of ethane to ethylene, J. Catal. 365 (2018) 14–23.
[10] R.W. Dorn, M.J. Ryan, T.-H. Kim, T.W. Goh, A. Venkatesh, P.M. Heintz, L. Zhou, W. Huang, A.J. Rossini, Identifying the molecular edge termination of exfoliated hexagonal boron nitride nanosheets with solid-state NMR spectroscopy and plane-wave DFT calculations, Chem. Mater. 32 (7) (2020) 3109–3121.
[11] R.W. Dorn, M.C. Cendejas, K. Chen, I. Hung, N.R. Altvater, W.P. McDermott, Z. Gan, I. Hermans, A.J. Rossini, Structure determination of boron-based oxidative dehydrogenation heterogeneous catalysts with ultrahigh field 35.2 T 11B solid-state NMR spectroscopy, ACS Catal. 10 (23) (2020) 13852–13866.
[12] W.-D. Lu, D. Wang, Z. Zhao, W. Song, W.-C. Li, A.-H. Lu, Supported boron oxide catalysts for selective and low-temperature oxidative dehydrogenation of propane, ACS Catal. 9 (9) (2019) 8263–8270.
[13] A.M. Love, M.C. Cendejas, B. Thomas, W.P. McDermott, P. Uchupalanun, C. Kruszynski, S.P. Burt, T. Agbi, A.J. Rossini, I. Hermans, Synthesis and characterization of silica-supported boron oxide catalysts for the oxidative dehydrogenation of propane, J. Phys. Chem. C. 123 (44) (2019) 27000–27011.
[14] B. Qiu, F. Jiang, W.-D. Lu, B. Yan, W.-C. Li, Z.-C. Zhao, A.-H. Lu, Oxidative dehydrogenation of propane using layered borosilicate zeolite as the active and selective catalyst, J. Catal. 385 (2020) 176–182.
[15] L. Cao, P. Dai, J. Tang, D. Li, R. Chen, D. Liu, X. Gu, L. Li, Y. Bando, Y.S. Ok, X. Zhao, Y. Yamauchi, A spherical superstructure of boron nitride nanosheets derived from boron-contained metal-organic frameworks, J. Am. Chem. Soc. 142 (19) (2020) 8755–8762.
[16] Y. Wang, W.-C. Li, Y.-X. Zhou, R. Lu, A.-H. Lu, Boron nitride wash-coated cordierite monolithic catalyst showing high selectivity and productivity for oxidative dehydrogenation of propane, Catal. Today 339 (2020) 62–66.
[17] M.C. Cendejas, R.W. Dorn, W.P. McDermott, E.A. Lebrón-Rodríguez, L.O. Mark, A.J. Rossini, I. Hermans, Controlled grafting synthesis of silica-supported boron for oxidative dehydrogenation catalysis, J. Phys. Chem. C. 125 (23) (2021) 12636–12649.
[18] P. Chaturbedy, M. Ahamed, M. Eswaramoorthy, Oxidative dehydrogenation of propane over a high surface area boron nitride catalyst: exceptional selectivity for olefins at high conversion, ACS Omega 3 (1) (2018) 369–374.
[19] J. Chen, P. Rohani, S. Karakalos, M.J. Lance, T.J. Toops, M.T. Swihart, E. Kyriakidou, Boron-hyperdoped silicon for the selective oxidative dehydrogenation of propane to propylene, Chem. Commun. 56 (2020) 9882–9885.
[20] Q. Liu, Y. Wu, F. Xing, Q. Liu, X. Guo, C. Huang, B2O3@BPO4 sandwich-like hollow spheres as metal-free supported liquid-phase catalysts, J. Catal. 381 (2020) 599–607.
[21] H. Zhou, X. Yi, Y. Hui, L. Wang, W. Chen, Y. Qin, M. Wang, J. Ma, X. Chu, Y. Wang, X. Hong, Z. Chen, X. Meng, H. Wang, Q. Zhu, L. Song, A. Zheng, F.-S. Xiao,

Isolated boron in zeolite for oxidative dehydrogenation of propane, Science 372 (2021) 76–80.
[22] N. Altvater, R. Dorn, M. Cendejas, W. McDermott, B. Thomas, A. Rossini, I. Hermans, B-MWW zeolite: the case against single-site catalysis, Angew. Chem. Int. Ed. 59 (2020) 6546–6550.
[23] C. Fild, D.F. Shantz, R.F. Lobo, H. Koller, Cation-induced transformation of boron-coordination in zeolites, Phys. Chem. Chem. Phys. 2 (13) (2000) 3091–3098.
[24] D. Massiot, F. Fayon, M. Capron, I. King, S. Le Calvé, B. Alonso, J.-O. Durand, B. Bujoli, Z. Gan, G. Hoatson, Modelling one- and two-dimensional solid-state NMR spectra, Magn. Reson. Chem. 40 (1) (2002) 70–76.
[25] D.E. Mears, Diagnostic criteria for heat transport limitations in fixed bed reactors, J. Catal. 20 (1971) 127–131.
[26] X. Fan, D. Liu, X. Sun, X. Yu, D. Li, Y. Yang, H. Liu, J. Diao, Z. Xie, L. Kong, X. Xiao, Z. Zhao, Mn-doping induced changes in Pt dispersion and PtxMny alloying extent on Pt/Mn-DMSN catalyst with enhanced propane dehydrogenation stability, J. Catal. 389 (2020) 450–460.
[27] J.C. Jansen, R. de Ruiter, E. Biron, H. van Bekkum, Isomorphous substitution of Si in zeolite single crystals. Part II. On the boron distribution and coordination in [B]-ZSM-5, Stud. Surf. Sci. Catal. 49 (1989) 679–688.
[28] M.B. Sayed, A. Auroux, J.C. Védrine, The effect of boron on ZSM-5 zeolite shape selectivity and activity II. Coincorporation of aluminium and boron in the zeolite lattice, J. Catal. 116 (1989) 1–10.
[29] J. Tian, J. Tan, M. Xu, Z. Zhang, S. Wan, S. Wang, J. Lin, Y. Wang, Propane oxidative dehydrogenation over highly selective hexagonal boron nitride catalysts: the role of oxidative coupling of methyl, Sci. Adv. 5 (3) (2019) eaav8063.
[30] X. Zhang, R. You, Z. Wei, X. Jiang, J. Yang, Y. Pan, P. Wu, Q. Jia, Z. Bao, L. Bai, M. Jin, B. Sumpter, V. Fung, W. Huang, Z. Wu, Radical chemistry and reaction mechanisms of propane oxidative dehydrogenation over hexagonal boron nitride catalysts, Angew. Chem. Int. Ed. 59 (2020) 8042–8046.
[31] P.V. Wiper, J. Amelse, L. Mafra, Multinuclear solid-state NMR characterization of the Brønsted/Lewis acid properties in the BP HAMS-1B (H-[B]-ZSM-5) borosilicate molecular sieve using adsorbed TMPO and TBPO probe molecules, J. Catal. 316 (2014) 240–250.
[32] H. Koller, C. Fild, R.F. Lobo, Variable anchoring of boron in zeolite beta, Micropor. Mesopor. Mat. 79 (1–3) (2005) 215–224.
[33] R. Millini, G. Perego, G. Bellussi, Synthesis and characterization of boron-containing molecular sieves, Top. Catal. 9 (1999) 13–34.
[34] S. Kroeker, J.F. Stebbins, Three-coordinated boron-11 chemical shifts in borates, Inorg. Chem. 40 (2001) 6239–6246.
[35] F. Yi, Y. Chen, Z. Tao, C. Hu, X. Yi, A. Zheng, X. Wen, Y. Yun, Y. Yang, Y. Li, Origin of weak Lewis acids on silanol nests in dealuminated zeolite Beta, J. Catal. 380 (2019) 204–214.
[36] H. Koller, C.-Y. Chen, S.I. Zones, Selectivities in post-synthetic modification of borosilicate zeolites, Top. Catal. 58 (7–9) (2015) 451–479.
[37] S.-J. Hwang, C.-Y. Chen, S.I. Zones, Boron sites in borosilicate zeolites at various stages of hydration studied by solid state NMR spectroscopy, J. Phys. Chem. B 108 (2004) 18535–18546.
[38] Y. Zhang, L. Qi, A. Lund, P. Lu, A.T. Bell, Mechanism and kinetics of acetone conversion to isobutene over isolated Hf sites grafted to silicalite-1 and SiO2, J. Am. Chem. Soc. 143 (22) (2021) 8352–8366.
[39] J. Datka, Z. Piwowarska, OH groups in boralites, J. Chern. Soc. Faraday Trans. 1 (85) (1989) 837–841.
[40] L.-Y. Zhao, J.-Y. Chen, W.-C. Li, A.-H. Lu, B2O3: A heterogeneous metal-free Lewis acid catalyst for carbon dioxide fixation into cyclic carbonates, J. CO2 UTIL. 29 (2019) 172–178.
[41] L.Y. Zhao, X.L. Dong, J.Y. Chen, A.H. Lu, A mechanochemical-assisted synthesis of boron, nitrogen co-doped porous carbons as metal-free catalysts, Chem. Eur. J. 26 (9) (2020) 2041–2050.
[42] J. Datka, Z. Piwowarska, The properties of boralites studied by infrared spectroscopy, J. Chern. Soc. Faraday Trans. 1 (85) (1989) 47–53.
[43] G. Coudurier, J.C. Vdrine, Catalytic and acidic properties of boron pentasil zeolites, Pure Appl. Chem. 58 (1986) 1389–1396.
[44] G. Liu, Z.-J. Zhao, T. Wu, L. Zeng, J. Gong, Nature of the active sites of VOx/Al2O3 catalysts for propane dehydrogenation, ACS Catal. 6 (8) (2016) 5207–5214.
[45] L. Shi, Y. Wang, B. Yan, W. Song, D. Shao, A.-H. Lu, Progress in selective oxidative dehydrogenation of light alkanes to olefins promoted by boron nitride catalysts, Chem. Commun. 54 (78) (2018) 10936–10946.